Journal of Materials Chemistry B

PAPER

View Article Online
View Journal

Cite this: DOI: 10.1039/c7tb01233k

Breaking the reduced glutathione-activated antioxidant defence for enhanced photodynamic therapy†

Qi-chen Zhan,‡[a] Xian-qing Shi,‡[a] Xiao-hong Yan,[a] Qian Liu,[b] Jia-hong Zhou,[a] Lin Zhou *[a] and Shao-hua Wei *[a]

Received 6th May 2017,
Accepted 12th July 2017

DOI: 10.1039/c7tb01233k

rsc.li/materials-b

Photodynamic therapy (PDT) has been applied in cancer treatment by utilizing reactive oxygen species (ROSs) to kill cancer cells. However, a high concentration of reduced glutathione (GSH) is present in cancer cells and can consume ROSs and sharply reduce the PDT activity. To address this problem, herein, we synthesized a thymine modified Zn phthalocyanine (ZnPc, a monomer and an active form for PDT) and prepared its nanoparticle form (an aggregator and an inactive form) with Hg^{2+} providing the driving force for the "thymine–Hg^{2+}–thymine" interaction. The nanoparticles could remain in the inactive form during the delivery process in blood. Once endocytosed by cancer cells, the nanoparticles are disintegrated, and deprived of Hg^{2+} by intracellular GSH, which decreases the level of GSH. Simultaneously, the activity of the released monomer ZnPc is recovered and high PDT activity is observed.

Introduction

PDT is a clinically used, minimally invasive therapeutic modality for cancer treatments.[1] In PDT, photosensitizers (PSs), accumulating in tumours, are activated by light of a specific wavelength to generate ROSs, such as singlet oxygen ($^1O_2$), to kill cancer cells.[2] So, PDT is based on PS-mediated oxidative cytotoxicity.[3]

GSH is an important antioxidant defence of cells because it can prevent the damage caused by ROSs. The stable ratio balance of GSH and oxidized glutathione (GSSH), defined as glutathione-redox homeostasis, is a critical regulator for the cellular redox state balance; and changes in GSH/GSSG are closely associated with cellular apoptosis processes.[4,5] An increase in GSH/GSSG is indicative of augmented antioxidant capacity, whereas a decrease is suggestive of oxidative stress and diminished antioxidant defences.[4] So, disturbing cellular glutathione-redox homeostasis could ultimately lead to cell toxicity or apoptosis.

Intracellular GSH concentration (*ca.* 10 mM) is known to be substantially higher than the extracellular levels (*ca.* 2 mM). Besides, the intracellular GSH concentration is reportedly higher in cancer cells, especially in chemo-resistant cancer cells, than in normal cells.[6–8] Recent reports indicated that the high level of GSH in cancer cells could consume ROS and sharply reduce PDT activity.[9] So, finding effective methods to reduce the GSH concentration and disrupt the glutathione-redox homeostasis inside cells might greatly improve PDT activity. But, the high GSH concentration in cancer cells could also be utilized for selective drug release and activation inside cancer cells.[10,11]

Thymine can form a "thymine–Hg^{2+}–thymine" complex with Hg^{2+}. GSH can deprive the complex of Hg^{2+} and lead to its disaggregation because of the higher affinity of GSH to Hg^{2+} than that of thymine. GSH–Hg^{2+} complex formation could decrease the free GSH concentration, destroy the glutathione-redox homeostasis and break the antioxidant defences of cells. Based on this concept, we synthesized thymine modified ZnPc (a monomer and an active form for PDT) and prepared its nanoparticle form (ZHNP, an aggregator and an inactive form; aggregation of ZnPc causes it to lose its PDT activity[12]) with Hg^{2+} providing the driving force for the "thymine–Hg^{2+}–thymine" interaction.

As shown in Scheme 1, ZHNP could maintain an inactive form during the delivery process in blood. Once endocytosed by cancer cells, the nanoparticles are disintegrated, and deprived of Hg^{2+} by intracellular GSH, which leads to a decrease in the level of GSH and breaks the endogenous antioxidant defence. Simultaneously, the activity of the released monomer ZnPc3 was recovered and showed high PDT activity in the low auto-oxidation microenvironment (Scheme 1).

[a] College of Chemistry and Materials Science, Jiangsu Key Laboratory of Biofunctional Materials, Jiangsu Collaborative Innovation Centre of Biomedical Functional Materials, Key Laboratory of Applied Photochemistry, Nanjing Normal University Nanjing (210023), P. R. China. E-mail: zhoulin@njnu.edu.cn, shwei@njnu.edu.cn; Tel: +86-025-8589-1761

[b] Department of Neurology, Jinling Hospital, Medical School of Nanjing University 305 East Zhongshan Road, Nanjing, Jiangsu (210002), P. R. China

† Electronic supplementary information (ESI) available. See DOI: 10.1039/c7tb01233k

‡ The authors contributed equally to this work.

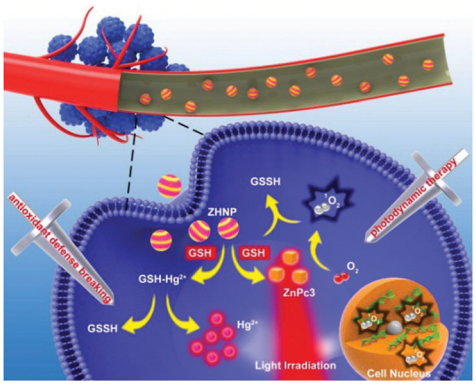

Scheme 1 Schematic presentation of the enhanced PDT effect of ZHNP by breaking the endogenous strong antioxidant defence.

Experiment

Chemicals

The chemicals used were of analytical purity grade and obtained from commercial suppliers and used without further purification unless otherwise stated. 1,8-diazabicyclo [5,4,0]-undec-7-ene (DBU), thymine-1-acetic acid and dicyclohexylcarbodiimide (DCC) were purchased from Sigma-Aldrich. TLC was performed on silica gel GF254 plates. 300–400 mesh silica gel was used for preparative column chromatography. The Glutathione Assay Kit and the Annexin V-FITC/PI apoptosis detection Kit were purchased from Beyotime Biotechnology. Dulbecco's minimum essential medium (DMEM) and fetal bovine serum (FBS) were from Gibco. Hoechst 33342 and the ROS detection kit (DCFH-DA) were from Beyotime. 3-[4,5-Dimethylthiazol-2-yl]-2,5-diphenyl tetrazoliumbromide (MTT) was from Amresco.

IR spectra were recorded on a Nicolet Nexus 670 IR-Spectrometer. ^{1}H NMR and ^{13}C NMR spectra were recorded using a Bruker Advance 400 MHz NMR spectrometer. Mass spectra were obtained on an UltrafleXtreme MALDI-TOF-MS spectrometer. Elemental analysis was performed using a Vario MICRO Elementar. Fluorescence spectra were carried out using a Perkin Elmer LS 50B fluorescence spectrophotometer. UV-Vis spectra were recorded on a Cary 50, Varian spectrophotometer. Cell morphology changes were observed under a Nikon Ti Observer fluorescence microscope. Transmission electron microscope (TEM) measurements were made on a JEOL JEM-2100F transmission electron microscope operated at an accelerating voltage of 200 kV.[13] Flow Cytometry (FCM), a rapid, accurate and objective detection technology for single particles usually used for assigning cells, was used to detect a variety of characteristics (parameters) of the particles and for qualitative and quantitative analysis. The electrochemical tests were performed using a CHI 660 C electrochemical analyser (CH Instruments, Shanghai, Chenhua Co.) at 30 ± 1 °C. A standard three-electrode system (consisting of a saturated calomel reference electrode (SCE), a catalyst modified glassy carbon electrode as the working electrode, and platinum wire as the auxiliary electrode) was used to perform electrochemical experiments.[14,15] A 665 nm LED (7 W) was used as the light source.

Synthesis of compounds

All the compounds were detected by melting point (M.P.) analysis, infrared spectra (IR), spectral imaging of hydrogen (^{1}H NMR) and an UltrafleXtreme MALDI-TOF-MS spectrometer. The synthetic route of all compounds is shown in Scheme 2.

Synthesis of 4-(three benzene methyl amino) phenol

A mixture of 4-(aminomethyl) phenol (500 mg, 4.06 mmol) and triethylamine in DMF (5 mL) was stirred under nitrogen at room temperature. Then, triphenylmethyl chloride (1.70 g, 6.09 mmol) in CH_2Cl_2 (25 mL) was added dropwise to the solution over a period of 3 h, and stirring was continued overnight after the titration was complete. The formed solid material was filtered off and washed with CH_2Cl_2 (3 × 25 mL) three times, and the filtrate was dried with sodium sulfate for 4 h. After filtration, the crude product was separated and purified by silica gel column chromatography using ethyl acetate/petroleum ether (1 : 5, v/v) as the eluent to obtain compound 1 as a sallow solid (1.11 g, 75%). M.P. 148 °C. IR (KBr, cm^{-1}): 3529 (OH), 3431 (NH), 3056 (Ar-H), 2813, 1607, 1512, 1447, 1245, 757; ^{1}H NMR (400 MHz, $CDCl_3$): δ (ppm) 7.67 (t, 6H, J = 4.2 Hz, Ar-H), 7.41–7.34 (m, 8H, Ar-H), 7.32–7.27 (m, 5H, Ar-H), 3.37 (s, 2H, CH_2), 2.16 (s, 1H, NH). ^{13}C NMR (100 MHz, d_6-DMSO): δ (ppm) 156.5, 146.6, 131.5, 129.1, 128.9, 128.2, 126.6, 115.4, 71.0, 47.3. Anal. calcd for $C_{26}H_{23}NO$: C, 85.45; H, 6.34; N, 3.83. Found: C, 85.40; H, 6.35; N, 3.81.

Synthesis of 4,5-(4-((three benzene methyl amino) methyl) phenoxy) phthalic nitrile

4,5-Dichlorophthalonitrile (100 mg, 0.507 mmol), compound 1 (741.9 mg, 2.03 mmol) and finely dried K_2CO_3 (561.2 mg, 4.06 mmol) were mixed in DMF (8 mL) under nitrogen and

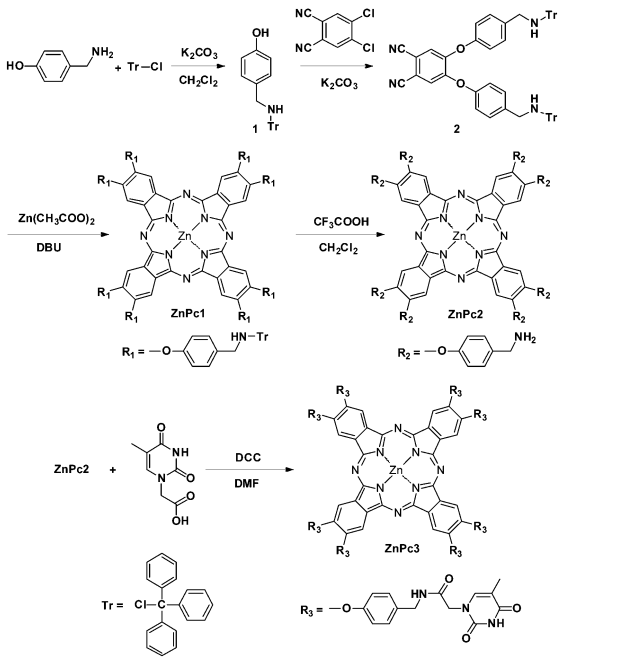

Scheme 2 Brief synthetic route for the synthesis of phthalocyanine derivatives.

stirred at 75 °C for 24 h. During the whole process, the reaction was monitored by TLC using ethyl acetate/petroleum ether (1 : 5, v/v). After cooling to room temperature, the solution was poured into water (50 mL) and a little HCl was added into the above solution. After filtration, the white precipitate was purified by column chromatography with silica gel as the column material to obtain compound 2 as a white solid. Yield: 350 mg (80.6%). M.P. > 200 °C. IR (KBr, cm^{-1}): 3435 (NH), 3059 (Ar-H), 2231 (CN), 1592, 1497, 1307, 1216 (C–O–C), 893, 706; ^{1}H NMR (400 MHz, $CDCl_3$): δ (ppm) 7.62–7.59 (m, 13H, Ar-H), 7.53 (d, 4H, J = 8.4 Hz, Ar-H), 7.37–7.32 (m, 13H, Ar-H), 7.28–7.24 (m, 6H, Ar-H), 7.11–7.08 (m, 4H, Ar-H), 3.43 (s, 4H, CH_2), 2.94 (d, 2H, J = 25.2 Hz, NH). ^{13}C NMR (100 MHz, $CDCl_3$): δ (ppm) 152.7, 152.1, 145.9, 139.0, 130.0, 128.7, 128.0, 127.9, 126.5, 121.5, 120.0, 110.1, 71.1, 47.3. Anal. calcd for $C_{60}H_{46}N_4O_2$: C, 84.28; H, 5.42; N, 6.55. Found: C, 84.32; H, 5.40; N, 6.57.

Synthesis of 2,3,9,10,16,17,23,24-8-(((amino)methyl)phenoxy)zinc phthalocyanine (ZnPc2)

Under a nitrogen atmosphere, a mixture of compound 2 (390 mg, 0.46 mmol), $Zn(CH_3COO)_2$ (52.3 mg, 0.29 mmol) and DBU (0.35 mL, 2.67 mmol) in *n*-pentanol (10 mL) was heated at 140 °C for 12 h. After cooling to room temperature, the solution was poured into CH_3OH (30 mL) to afford a crude green solid. The deep blue solid product was precipitated and collected by filtration, then washed with methanol until the filtrate was colourless. The blue fraction was collected, evaporated under vacuum, and dried at 50 °C for 12 h to afford the product as a dark green solid (ZnPc1).

ZnPc1 (500 mg, 0.14 mmol) was dissolved in CH_2Cl_2 (25 mL), and trifluoroacetic acid (TFA) (2 mL) was added in excess. The solution was stirred at room temperature for 3 h. After green solid precipitation and filtration, the cake was washed with CH_2Cl_2. Thereafter, the green solid was dissolved in water and precipitated by adjusting the pH to 8–9. After filtration, the product was vacuum-dried to afford ZnPc2 as a dark green solid. Yield: 177 mg (80.1%). M.P. > 200 °C. IR (KBr, cm^{-1}): 3425 (NH_2), 2852 (CH_2), 1599 (NH_2), 1498, 1268 (C–O–C), 1090, 887; ^{1}H NMR (400 MHz, d_6-DMSO): δ (ppm) 7.52–6.99 (m, 40H, Pc-H, Ar-H), 4.05 (s, 16H, CH_2). MS (MALDI-TOF, $[M + H]^+$) m/z: calcd for $C_{88}H_{72}N_{16}O_8Zn$: 1544.5. Found: $[M + H]^+$ 1545.5. Anal. calcd for $C_{88}H_{72}N_{16}O_8Zn$: C, 68.32; H, 4.69; N, 14.49. Found: C, 68.35; H, 4.67; N, 14.51.

Synthesis of 2,3,9,10,16,17,23,24-8-((((thymine-1-acetic acid)amino)methyl)phenoxy) zinc phthalocyanine (ZnPc3)

As shown in Scheme 2, ZnPc3 was synthesized according to a typical DCC condensation method. 50 mg (0.03 mmol) of ZnPc2 and 66 mg (0.36 mmol) of thymin-1-ylacetic acid were dissolved in DMF (8 mL). Then, 64 mg (0.3 mmol) of DCC was added in one portion, and the reaction mixture was stirred at room temperature for 24 h. The precipitate was removed by centrifugation after the material reaction was complete, the centrifugal supernatant fluid was poured into water and the crude product precipitated. Then, the resulting solid was washed with distilled water and methanol, respectively, and dried under vacuum at 60 °C; a grass green solid was obtained successfully (ZnPc3). Yield: 68 mg (73.1%). M.P. > 200 °C. IR (KBr, cm^{-1}): 3461, 3325 (NH), 2928, 2850 (Ar-H), 1686 (C═O), 1645 (C═C), 1380, 1238 (C–O–C), 795; ^{1}H NMR (400 MHz, d_6-DMSO): δ (ppm) 8.50 (s, 8H, NH), 8.08 (s, 8H, Ar-H), 7.95–7.14 (m, 40H, Pc-H, Ar-H), 5.76 (d, 16H, J = 8 Hz, CH_2), 4.25 (s, 16H, CH_2), 3.89 (s, 24H, CH_3). MS (MALDI-TOF, $[M + H]^+$) m/z: calcd for $C_{144}H_{120}N_{32}O_{32}Zn$: 2876.07. Found: $[M + H]^+$ 2876.30. Anal. calcd for $C_{144}H_{120}N_{32}O_{32}Zn$: C, 60.14; H, 4.21; N, 15.58. Found: C, 61.05; H, 4.34; N, 15.21.

ZHNP preparation

100 μL of ZnPc3 (2.0 μM, in DMF) and 100 μL of $HgSO_4$ solution (16.0 μM, in ethanol) were mixed in methanol. The mixture was stirred for 30 min to form ZHNP. The resulting ZHNP was purified by dialysis of the solution using a 12–14 kDa cut-off cellulose membrane for 24 h.

$^1O_2$ detection

$^1O_2$, an important indicator of the photosensitizing ability of PSs in PDT, results from the energy transfer between the triplet state of photosensitizers and the ground state of molecular oxygen.[16–18] ADPA was used as the scavenger to evaluate the singlet oxygen generation ability of the compounds in water. ADPA can interact with $^1O_2$ to generate its endoperoxide and induce a decrease of its absorbance intensity (λ_{max} of ADPA = 378 nm). 3 mL of PS solution was mixed with 150 μL ADPA (5.5 mM). We monitored $^1O_2$ generation by detecting the characteristic peak intensity change of ADPA in water locating at 378 nm under 665 nm LED (7 W) irradiation. The rate of $^1O_2$ formation was calculated using the following equation:

$$\ln([ADPA]_t/[ADPA]_0) = -kt$$

where $[ADPA]_t$ and $[ADPA]_0$ are the concentrations of ADPA after and prior to irradiation, respectively.

In vitro glutathione-redox environment detection

The glutathione-redox balance, expressed as the ratio of intracellular reduced GSH and GSSH, plays an important role in regulating cell function.[19] For the detection of *in vitro* total GSH and GSSH, a total glutathione assay kit was used. Glutathione reductase can reduce GSSG into GSH, then GSH reacts with a chromogenic substrate DTNB, and produces yellow TNB and GSSG. All glutathione determines the amount of yellow TNB formed, thus by measuring A_{405} the amount of total glutathione can be calculated.

Dark cytotoxicity

In the dark toxicity test, A549 cells were seeded into 96 well plates at a density of 5×10^5 cells per cm^2 and incubated for 24 h in an incubator.[20–22] After that, the cells were treated with ZnPc3 (5.0 μM), Hg^{2+} (20.0 μM) or ZHNP (5.0 μM, the concentration of ZHNP was defined by ZnPc3 in the complex) for another 24 h. Then, cellular survival was measured by the [3-(4,5-dimethylthiazol-2-yl)-2,5-diphenyltetrazolium bromide] (MTT) colorimetric assay.

Phototoxicity studies

For the determination of light-dependent cytotoxicity, A549 cells were seeded into 96 well plates at a density of 5×10^5 cells per cm^2 and incubated for 24 h. Then, the cells were treated with ZnPc3 (5.0 μM), Hg^{2+} (20.0 μM) or ZHNP (5.0 μM, the concentration of ZHNP was defined by ZnPc3 in the complex) for another 4 h. After that, the cells were washed with PBS three times to remove adhered ZnPc. Then, the cells were exposed to light for 5 min. The cells were incubated for 24 h and cell viability was measured by MTT assay.[23,24] In addition, the apoptosis properties of the drugs were determined using an Annexin V/FITC-PI apoptosis detection kit and detected using a flow cytometer.

Hoechst 33342 staining

Nuclear staining is a usual method to detect chromatin condensation by Hoechst 33342.[25] After treating with drugs overnight and irradiating with light, the cells were washed with phosphate buffered saline (PBS) three times and treated with 25 μg mL^{-1} Hoechst 33342 at 37 °C with 5% CO_2 in the dark for 30 min.[26] Then, a fluorescence microscope was used to observe the change of nuclear morphology.

Statistical analysis

All biochemical experiments were performed in duplicate and an average of the results was used. Statistical analysis was done and the mean, standard deviation, standard error, and significant changes were expressed as the mean ± SD. $P < 0.05$ was considered to be statistically significant.

Results and discussion

Morphology and aggregation properties of ZHNP

The TEM images to elucidate the aggregation process between ZnPc3 and Hg^{2+} are shown in Fig. 1. After adding Hg^{2+}, ZnPc3 immediately forms aggregates with Hg^{2+} at a low aggregation degree.

Then, the morphology of the complex changed to the floc form after 1 h, indicating their increased aggregation degree. With the increase of reaction time, ZnPc3 aggregated gradually and formed ZHNP, which could stably disperse in aqueous solution for a long time.

Further evidence for the aggregation process between ZnPc3 and Hg^{2+} was obtained from the UV-Vis absorption (Fig. 2A) and fluorescence spectra (Fig. 2B). There are two absorbance bands of ZnPc3 in the region from 550 to 750 nm. The aggregator form band of ZnPc3 was located at 630 nm and the monomer one was at 685 nm. After forming ZHNP, the monomer band was sharply decreased but the aggregator band was increased, which indicates that Hg^{2+} could interact with the thymine of ZnPc3 and such interaction could induce its aggregation. Additional evidence of ZnPc3 aggregation behaviour triggered by Hg^{2+} was obtained from the fluorescence intensity change in the complex system. It is well-known that monomeric Pc has a strong fluorescence signal, whereas the aggregated form does not. So, fluorescence signal detection is a sensitive method

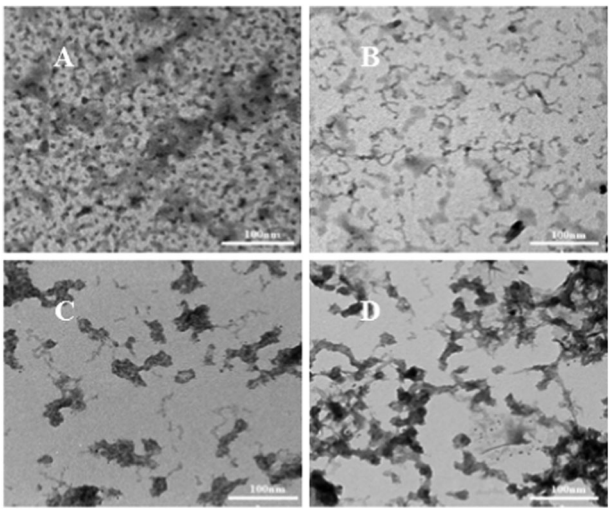

Fig. 1 The TEM image of the ZHNP formation process by mixing ZnPc3 and Hg^{2+} (A) for 0 h, (B) for 1 h, (C) for 2 h and (D) for 3 h (bar = 100 nm).

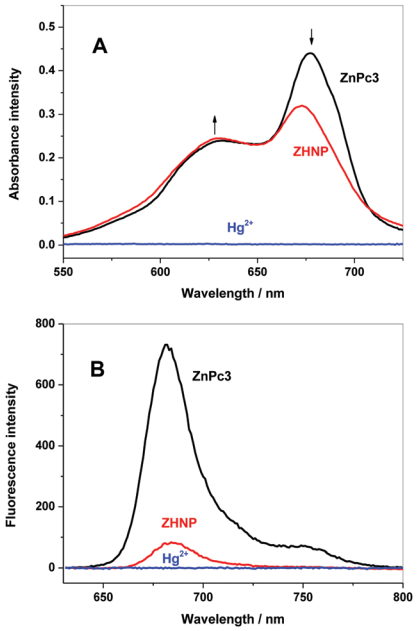

Fig. 2 (A) Absorption spectra of ZnPc3, Hg^{2+} and ZHNP; (B) fluorescence spectra of ZnPc3, Hg^{2+} and ZHNP (λ_{ex} = 610 nm).

to investigate the aggregation of Pcs because the formation of ZnPc3 aggregates results in dramatic fluorescence quenching.[27] As shown in Fig. 2B, ZnPc3 shows a strong fluorescence signal at 698 nm. The formation of ZHNP results in an obvious fluorescence quenching of ZnPc3, which is consistent with the TEM and UV-Vis absorption spectra results.

To further verify that the interaction of "thymine–Hg^{2+}–thymine" is the driving force for the aggregation process between ZnPc3 and Hg^{2+}, experiments on the selectivity of ZnPc3 for different metal ions were carried out. Thymine is known as one of the most specific ligands for Hg^{2+} that can form a thymine–Hg–thymine complex with strong affinity and

high selectivity.[28,29] As an analogue of it, ZnPc3 combined with thymine-1-acetic acid may retain this selectivity. To investigate the selectivity of ZnPc3 to Hg^{2+}, the fluorescence of ZnPc3 in the presence of different metal ions, including Ba^{2+}, Co^{2+}, K^{+}, Al^{3+}, Mg^{2+}, Na^{+}, Zn^{2+}, Ni^{2+} and Fe^{3+}, was investigated under identical conditions. Fig. 3A shows that only Hg^{2+} leads to dramatic fluorescence quenching (about 79.3%), whereas other ions cause no obvious change. These results indicate that ZnPc3 has excellent selectivity to Hg^{2+}.

Electrochemical methods for the detection of the affinity between ZnPc3 and Hg^{2+} are shown in Fig. 3B. No obvious oxidation peak was detected in ZnPc3. Hg^{2+} showed two clear oxidation peaks. After forming ZHNP, the oxidation peak was obviously shifted, which indicated the complexation interaction between Hg^{2+} and ZnPc3. The selectivity of ZnPc3 for different metal ions and the electrochemical results all indicated that "thymine–Hg^{2+}–thymine" is the driving force for the aggregation process between ZnPc3 and Hg^{2+}.

GSH activated disaggregation and PDT activity recovery of ZHNP

Aggregation behaviour of Pcs always lowers their PDT activity.[12] So, we hypothesize that after forming ZHNP, the PDT activity of ZnPc3 could be greatly decreased, which could be helpful for ZHNP to maintain low toxicity during the delivery process in blood. However, we hoped that the activity of ZHNP could be recovered after its endocytosis by cancer cells. So, the disaggregation of ZHNP is important for the recovery of its PDT activity. Biological thiols, including cysteine (Cys), homocysteine (Hcy), and GSH, could deprive ZHNP of Hg^{2+} and lead to its disaggregation because of the higher affinity of biothiols to Hg^{2+} than that of thymine.[30]

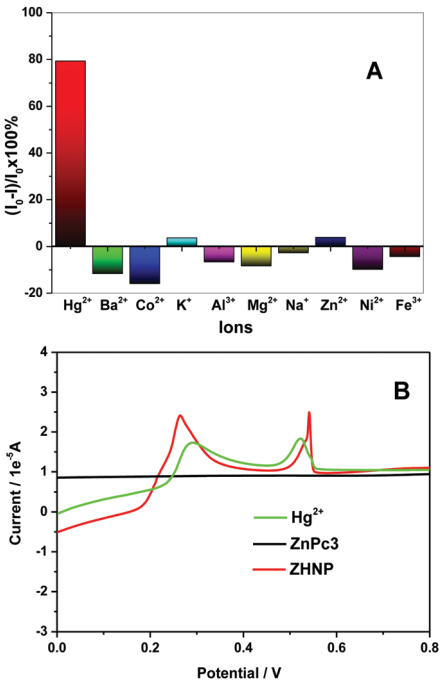

Fig. 3 (A) Fluorescence quenching ratio $(I_0 - I)/I_0$ at 680 nm after the addition of various kinds of metal ions. I_0 and I are the fluorescence intensity at 680 nm before and after the addition of metal ions. (B) Cyclic voltammograms of ZnPc3, ZHNP and Hg^{2+} in N_2-saturated solution at 50 mV s^{-1}.

Although Cys and Hcy could also cause the disaggregation of ZHNP, the intracellular content of Cys and Hcy is much lower than that of GSH.[31] So, we proposed that ZHNP could be disaggregated and recover its PDT activity triggered by GSH inside cancer cells because the intracellular GSH concentration (*ca.* 10 mM) is known to be substantially higher than the extracellular levels (*ca.* 2 mM) and the intracellular GSH concentration is reportedly higher in cancer cells than in normal cells.[6,7] Furthermore, ZnPc3 release, triggered by GSH, was accompanied by GSH–Hg^{2+} formation, which could cause GSH depletion and improve the PDT activity.

To verify the disaggregation of ZHNP by biothiols, fluorescence recovery and electrochemical experiments were carried out. The selectivity for ZHNP fluorescence recovery by various kinds of amino acids and GSH is shown in Fig. 4A. The addition of Cys, Hcy and GSH results in an obvious disaggregation of ZnPc3 with the recovery of fluorescence intensity since the Hg^{2+}–thymine interaction of ZHNP was replaced by the stronger Hg^{2+}–S bond between Hg^{2+} and biothiols, resulting in ZHNP disaggregation and fluorescence recovery.[28]

Electrochemical experiment results indicated that after GSH addition, the two clear oxidation peaks of ZHNP sharply decreased and such a phenomenon could be prevented by *N*-ethylmaleimide (NEM) (Fig. 4B), a kind of inhibitor to suppress the interaction of Hg^{2+} and GSH.[32] The above results all verified the disaggregation of ZHNP by biothiols.

In addition, the recovery of ZHNP PDT activity, triggered by biothiols, was analysed by comparing the $^1O_2$ generation ability before and after the addition of biothiols. $^1O_2$ is one of the most active ROSs and has a prominent role in various biological and chemical processes in PDT.[33–37] It occurs because of the energy transfer between the triplet state of PSs and the ground state of molecular oxygen during the PDT process. $^1O_2$ generation was detected using the ADPA bleaching method. As shown in Fig. 5A–D, the $^1O_2$ generation ability of ZnPc3 was sharply decreased after the formation of ZHNP. Adding biothiols obviously induced the recovery of the $^1O_2$ generation ability of ZHNP, which indicated that Hg–thymine interaction was replaced by the stronger Hg–S bond, and ZHNP disaggregates into the monomer active form again. To verify this hypothesis, their fluorescence spectra were detected. As we know, monomeric Pc has a strong fluorescence signal, whereas the aggregates do not. So, fluorescence signal detection is a sensitive method to investigate the aggregation of Pcs because the formation of the ZnPc aggregates results in dramatic fluorescence quenching and the formation of the ZnPc monomer results in fluorescence recovery.[27] These results indicated that Hg–thymine interaction was replaced by the stronger Hg–S bond, and ZHNP disaggregates into a monomer active form again. As shown in Fig. 5E, the addition of Hg^{2+} leads to a significant decrease in the fluorescence intensity but the addition of biothiols leads to fluorescence recovery. These results indicated that Hg–thymine interaction was replaced by the stronger Hg–S bond, and ZHNP disaggregates into the monomer active form again.

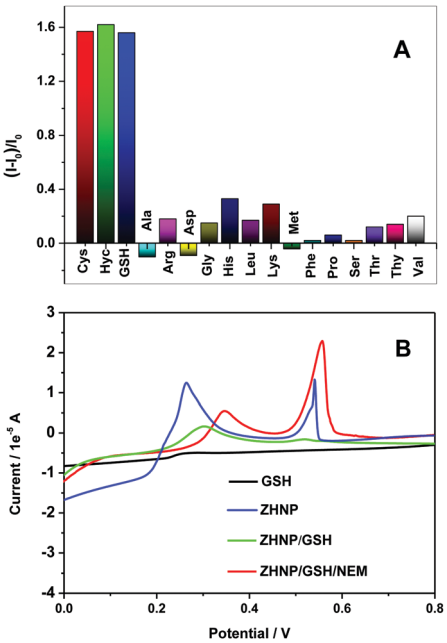

Fig. 4 (A) Fluorescence changing ratio $(I - I_0)/I_0$ of ZHNP at 682 nm after the addition of various of amino acids and GSH; (B) the metal mass-normalized cyclic voltammograms for GSH, ZHNP, ZHNP/GSH and ZHNP/GSH/NEM.

In vitro anticancer activity

The uptake of ZnPc3 and ZHNP in A549 cells is shown in Fig. 6A; the intracellular concentration shows no obvious difference within 4 h. As shown in Fig. 6B, before irradiation, ZnPc3, Hg^{2+} and ZHNP all showed low anticancer activity. On the contrary, after irradiation by 665 nm LED light for 5 min and incubation for another 24 h, the anticancer activity of ZnPc3 and ZHNP treated cells obviously increased (Fig. 6C).

Besides, the increasing degree of anticancer activity of ZHNP was much higher than the sum effect of ZnPc3 and Hg^{2+}, which implied that there are additive and synergistic anticancer mechanisms in the anticancer process of ZHNP. To elucidate the synergistic effect of ZHNP, the anticancer activity of ZnPc3 alone, Hg^{2+} alone, Hg^{2+} uptake first followed by ZnPc3, ZnPc3 uptake first and then Hg^{2+} uptake, and ZHNP was compared after irradiation. As shown in Fig. 6C, the increasing degree of anticancer activity of ZHNP was much bigger than the sum effect of ZnPc3 and Hg^{2+}, which indicated that there are additive and synergistic anticancer mechanisms in the anticancer process of ZHNP (synergistic index = 1.72, Table 1) (MGI, mean growth inhibition rate = growth rate of treated group/growth rate of untreated group). The synergistic index was calculated by dividing the expected growth inhibition rate by the observed growth inhibition rate. An index of more than 1 indicates a synergistic effect and an index <1 indicates less than an additive effect. On the contrary, although the other two groups (Hg^{2+} uptake first followed by ZnPc3 or ZnPc3 uptake first and then Hg^{2+} uptake) also showed improved anticancer activity compared with ZnPc3 or Hg^{2+} alone, their synergistic indexes were 0.87 and 0.96. Different from these two groups, ZHNP could ensure that ZnPc3 and Hg^{2+} could be taken up by cancer cells, simultaneously, and locate at the same position after being released inside cells. PDT is based on the irradiation of photosensitizers with an appropriate wavelength to generate ROSs, such as $^1O_2$ and free radicals, to oxidize various cellular compartments, finally resulting in irreversible damage of tumor cells. The life time of such ROSs is quite short, which indicates that their effective diffusion distance is short. Taking $^1O_2$ as an example, its life time is only 1 μs in aqueous solution and during this interval it can diffuse over a mean radial distance of only 100 nm. So, if Hg^{2+} could not destroy GSH around ZnPc3, its PDT activity could not be improved efficiently.

Apoptosis is a programmed or suicidal cell death, which plays an important role in maintaining the balance between cell proliferation and death. To evaluate the morphologic characteristics of apoptotic nuclei, the cells were stained with Hoechst 33342 after incubation with Hg^{2+}, ZnPc3, and ZHNP. As shown in Fig. 7, control cells exhibit homogeneous, weak and intact nuclear staining, and drug treated cells display typical apoptotic changes, such as stained brightness, reduction of nuclei volume and condensed chromatin, which indicated that Hg^{2+}, ZnPc3, and ZHNP can induce apoptosis.

To further verify that ZHNP could induce apoptosis, Annexin V-FITC/PI apoptosis detection was performed to compare the apoptosis-inducing capabilities of Hg^{2+}, ZnPc3 and ZHNP.

Annexin V-FITC labels the phosphatidylserine sites that translocate to the extracellular membrane upon initiation of apoptosis, while PI labels the intracellular DNA in the late apoptotic cells where the plasma membrane has been compromised. This combination allows the differentiation of early apoptotic cells, late apoptotic cells and viable cells, which can be quantitatively determined by flow cytometry.[38] The total apoptotic ratio of ZHNP was 69.31% obtained by the summation of the early apoptotic ratio of 33.64% and the late apoptotic ratio of 35.67%, which was much higher than 42.59% of ZnPc and 12.74% of Hg^{2+} (Fig. 8).

In vitro anticancer mechanism

Based on the above results, we conclude that the anti-cancer activity of ZHNP was superior to that of ZnPc3. We hypothesized that there were two anticancer mechanisms, PDT and glutathione-redox homeostasis dysfunction, in ZHNP and these mechanisms have additive and synergistic effects.

2,7-Dichlorodi-hydrofluorescein diacetate (DCFH-DA), a ROS fluorescent probe, can penetrate the cell membrane freely and can be oxidized into fluorescent DCF by ROS inside cells. So, the fluorescence intensity of DCF can indicate the oxidative stress level inside the cell.[39,40] In Fig. 9, cells treated with three drugs (ZnPc3, Hg^{2+} and ZHNP) showed different fluorescence intensities after trapping DCFH-DA. By comparison of the DCF fluorescence intensity inside the cells, we can conclude that the ROS generation ability of the drugs followed the order: ZHNP $>$ Hg^{2+} $>$ ZnPc3 (Fig. 10).

Hg^{2+} entering the cells could increase the generation of ROSs, which is a similar result to that reported.[41] The data indicated that ZHNP has stronger photodynamic anti-cancer

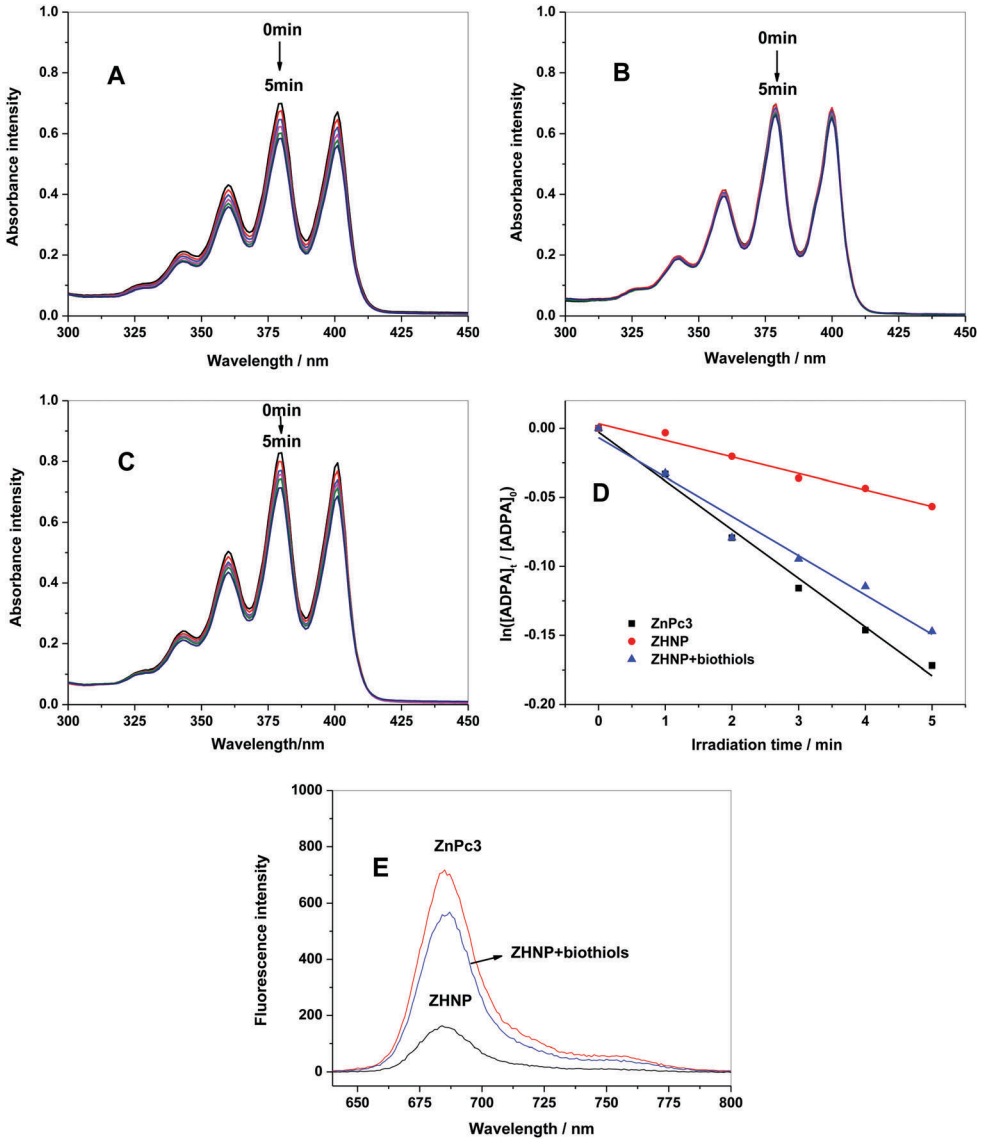

Fig. 5 Time-dependent bleaching of ADPA caused by $^1O_2$ generated by ZnPc3 (A), ZHNP (B) and ZHNP with biothiols (C) upon irradiation, monitored as a function of time. (D) The best fit of $^1O_2$ generation to the above experimental points. (E) Fluorescence spectra (λ_{ex} = 610 nm) of ZnPc3, ZHNP and ZHNP + biothiols.

activity than ZnPc3 because of its high ROS generation ability. And the disaggregation of ZHNP not only recovers but also improves its *in vitro* ROS generation ability. However, such an increase in ROSs might not only occur because of the light triggered PDT process, but also from GSH depletion.

GSH is an important antioxidant agent in cells. GSH can prevent the damage of cellular components by strong oxidizing ROSs. ROSs can be reduced by GSH, and GSH can be oxidized to GSSH by ROSs, simultaneously. Glutathione-redox balance, defined as the total amount of glutathione (GSH + GSSH) and the ratio of GSH/GSSG, is a critical regulator of the cellular redox state, and changes in the glutathione-redox balance are closely associated with cellular processes, such as proliferation and apoptosis.[4] A glutathione assay kit can detect the total glutathione (GSH + GSSH) and GSH concentration inside the cells. The original data of GSH, GSH + GSSH, GSSH and GSH/GSSH in ZnPc3, Hg^{2+} or ZHNP treated and control cells are listed in Table 2. As shown in Fig. 11A, the GSH amounts of ZnPc3, Hg^{2+} or ZHNP treated cells were sharply decreased compared with the control cells. Hg^{2+} could oxidize GSH to GSSH and ZnPc3 and light treated cells also showed an obvious decrease in the amount of GSH, which is possibly because GSH could be oxidized byROSs to GSSH. The GSH decreasing effect of ZHNP could be achieved by a combined effect of the above two processes.

Reports indicated that an increase in GSH/GSSG is indicative of augmented antioxidant capacity, whereas a decrease is suggestive of diminished antioxidant defences.[4] As showed in Table 2, the GSH/GSSH values of ZnPc3, Hg^{2+} and ZHNP were all greatly reduced compared with control cells. This result is suggestive of diminished antioxidant defences, which is very

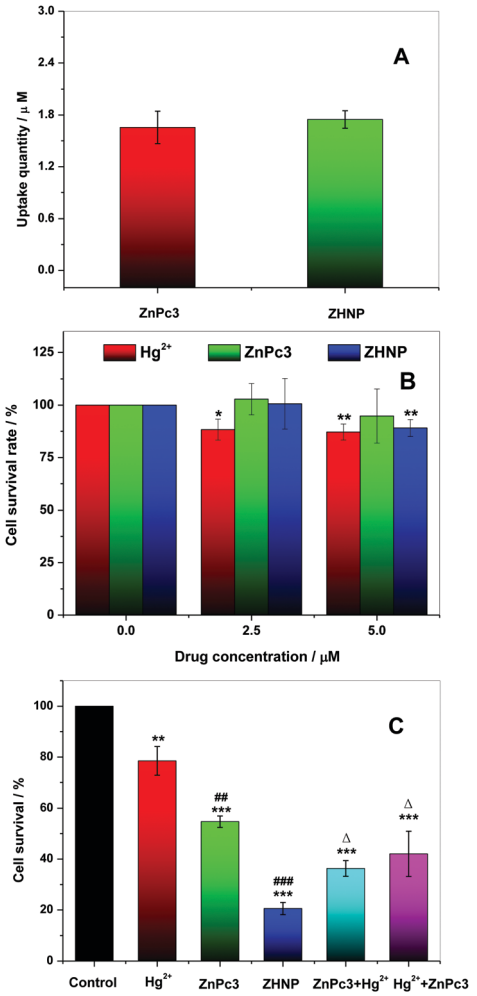

Fig. 6 (A) Cellular uptake quantity of ZnPc3 and ZHNP within 4 h. (B) Dark cell toxicity comparison of Hg^{2+}, ZnPc3 and ZHNP. (Data are expressed as means ± SD; $^{*}P < 0.05$; $^{**}P < 0.01$ *versus* control.) (C) Light toxicity comparison of Hg^{2+}, ZnPc3, ZHNP, ZnPc3 + Hg^{2+} and Hg^{2+} + ZnPc3. ($^{**}P < 0.01$; $^{***}P < 0.001$ *versus* control; $^{\#\#}P < 0.01$, $^{\#\#\#}P < 0.001$ *versus* Hg^{2+}; $^{\Delta}P < 0.05$ *versus* ZHNP; $^{\Delta}P < 0.05$, Hg^{2+} uptake first followed by ZnPc3 or ZnPc3 uptake first and then Hg^{2+} uptake *versus* ZHNP).

Table 1 Synergistic index of combined treatment with glutathione-redox dysfunction and PDT ($P < 0.001$ anticancer activity of ZHNP *vs.* ZnPc3 and Hg^{2+})

Additive and synergistic effect		
PDT treatment	Drug	ZnPc3
	MGI	45.92%
Glutathione-redox dysfunction	Drug	Hg^{2+}
	MGI	79.71%
Combination treatment	Drug	ZHNP
	Expected	36.60%
	Observed	21.32%
P-value		$P < 0.001$
Additive and synergistic effect index		1.72

helpful for the PDT process because PDT is an oxidation damage process. The degree to which ZHNP decreased the GSH/GSSH value was not as high as that of ZnPc3 or Hg^{2+}, but the total glutathione (GSH + GSSH) of ZHNP was greatly

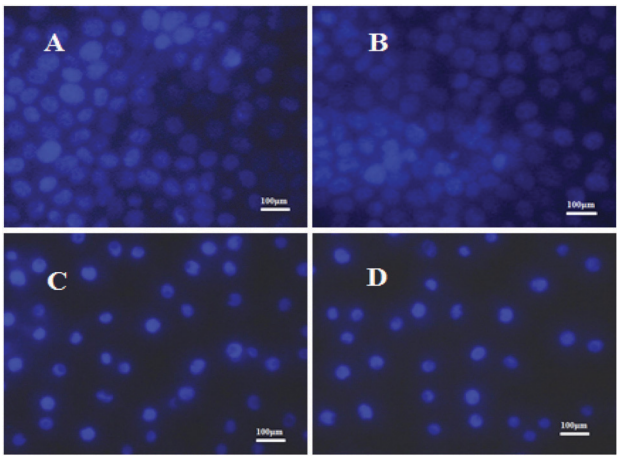

Fig. 7 Fluorescence micrographs of A549 cells stained with Hoechst 33342 (A) and treated with Hg^{2+} (B), ZnPc3 (C) and ZHNP (D) and light irradiation (bar = 100 μm).

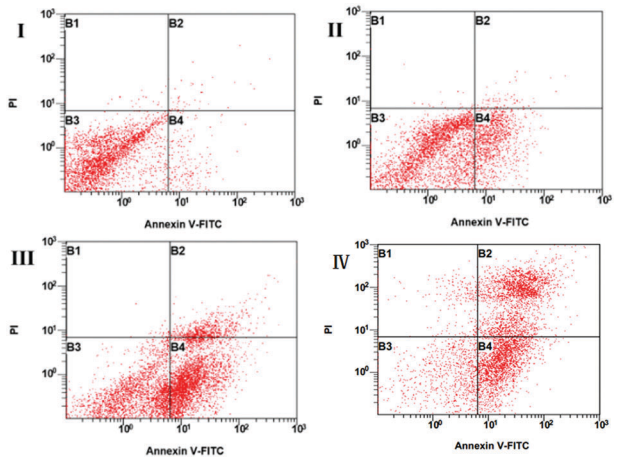

Fig. 8 Flow cytometric analysis of cell apoptosis induced by no drug (I: control), Hg^{2+}(II), ZnPc3(III) and ZHNP(IV) using Annexin V-FITC/PI staining. In each panel, the lower-left (B3, Annexin V-FITC^{-}, PI^{-}), lower-right (B4, Annexin V-FITC^{+}, PI^{-}) and upper-right (B2, Annexin V-FITC^{+}, PI^{+}) quadrants represent the populations of the viable, early apoptotic and late apoptotic cells, respectively.

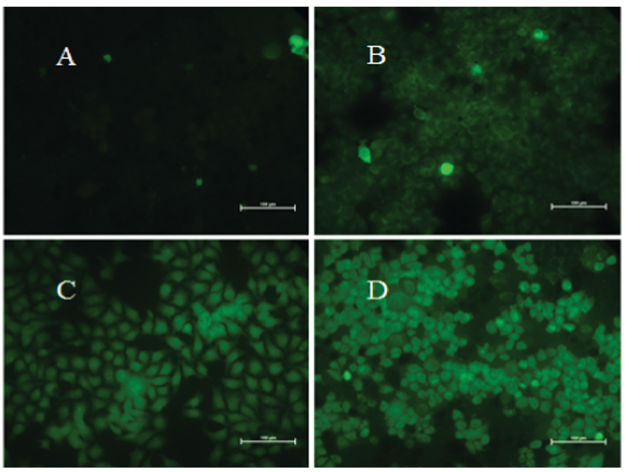

Fig. 9 Fluorescence signal of A549 stained with DCFH-DA. (A) Control cells; cells respectively treated with ZnPc3 (B), Hg^{2+} (C) and ZHNP (D) after irradiation and re-incubation for 4 h (bar = 100 μm).

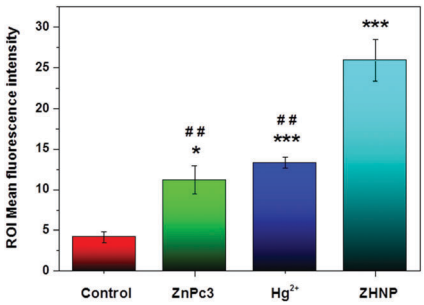

Fig. 10 Fluorescence micrographs of A549 stained with Hoechst 33342. (Control) Normal cells; cells respectively treated with Hg^{2+}, ZnPc3 and ZnPc3/Hg^{2+} 5 min of irradiation; bar = 100 μm. (Data are expressed as means ± SD; $^{*}P < 0.05$, $^{***}P < 0.001$ *vs.* control; control means that cells were treated without Drugs; $^{\#\#}P < 0.01$ *vs.* ZHNP).

Table 2 Comparison of the GSH + GSSH, GSH, GSSH, GSH/GSSH values of ZnPc3, Hg^{2+} and ZHNP with control cells

	Control	ZnPc3	Hg^{2+}	ZHNP
GSH + GSSH	21.04	20.52	20.88	7.84
GSH	16.32	9.58	10.72	5.71
GSSH	4.72	10.94	10.16	2.13
GSH/GSSH	3.47	0.88	1.06	2

decreased compared with ZnPc3 or Hg^{2+} treated cells (Fig. 11B). The possible reason for this phenomenon is that ROSs could destroy the enzymes necessary for the GSH metabolism pathway and lead to a decrease in the amount of GSH. These results indicated that ZHNP could break the glutathione-redox homeostasis more effectively.

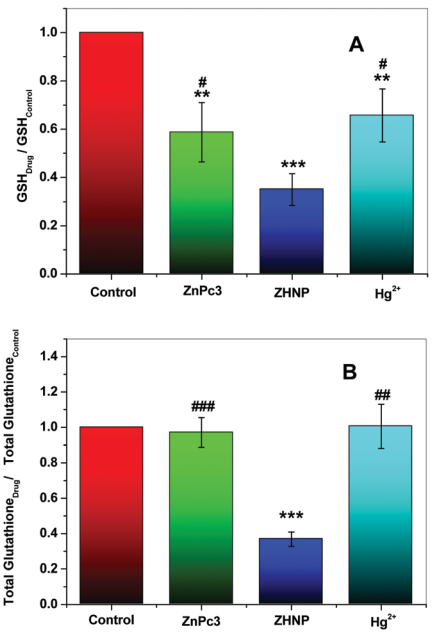

Fig. 11 (A) The GSH relative amount of drug and light treated cells; (B) the total glutathione (GSH + GSSH) relative amount of drug and light treated cells. ($^{**}P < 0.01$ $^{***}P < 0.001$, drug and light treated cells *versus* control; $^{\#\#}P < 0.01$, $^{\#\#\#}P < 0.001$ *vs.* ZHNP).

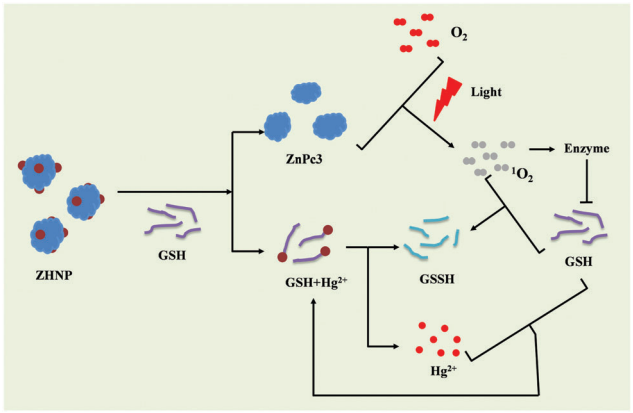

Scheme 3 Flow diagram of the enhanced PDT effect of ZHNP by breaking the endogenous strong antioxidant defence.

So, based on the above results, we can conclude that the anticancer mechanism of ZHNP is a combined effect of PDT and GSH depletion. After the inactive ZHNP was endocytosed by cancer cells, it was activated by GSH and release monomer ZnPc3 and GSH–Hg^{2+}. ZnPc3 could be triggered by light to generate ROSs to oxidize damaged cancer cells. And the ROSs generated in the PDT process could deplete GSH. In addition, the released Hg^{2+} could form a stable complex with GSH. This effect could reduce GSH concentration, break the glutathione-redox balance, and therefore, diminish the antioxidant defences of cells, and finally, greatly improve the PDT activity (Scheme 3).

Conclusions

In conclusion, to overcome the antioxidant defence in the cells during the PDT process, we have developed nanoparticles of ZnPc3 integrated with Hg^{2+} based on ''thymine–Hg^{2+}–thymine'' interaction. The inactive ZHNP could simultaneous release the active monomer ZnPc and decrease the GSH level for highly efficient PDT.

Some people may think that mercury could be dangerous to human health.[42] But in this system, the mercury concentration was low and a single Hg^{2+} ion had weak toxicity under our experimental conditions. Similarly, arsenic trioxide (As_2O_3), which was proposed as a toxin and a carcinogen, has recently been recognized as one of the most effective drugs for the treatment of acute promyelocytic leukemia.[43] The drug dose and tumour selectivity of these drugs are very important for cancer treatment. Thus, the potential of using mercury as an antioxidant defence destroyer for improving the PDT activity has been demonstrated.

Acknowledgements

This research was financially supported by the National Natural Science Foundation of China (No. 21571105 and 21671105), the program of natural science research of Jiangsu higher education institutions of china (15KJB150013), the project BK20161554 supported by NSF of Jiangsu Province of China, the Priority Academic

Program Development of Jiangsu Higher Education Institutions (PAPD), and the Foundation of Jiangsu Collaborative Innovation Centre of Biomedical Functional Materials (161090H001).

Notes and references

1 X. Duan, C. Chan, N. Guo, W. Han, R. R. Weichselbaum and W. Lin, *J. Am. Chem. Soc.*, 2016, **138**, 16686–16695.
2 J. Park, Q. Jiang, D. Feng, L. Mao and H. C. Zhou, *J. Am. Chem. Soc.*, 2016, **138**, 3518–3525.
3 M. C. Luna, A. Ferrario, S. Wong, A. M. R. Fisher and C. J. Gomer, *Cancer Res.*, 2000, **60**, 1637–1644.
4 Y. Zhou, D. E. Harrison, K. Love-Myers, Y. Chen, A. Grider, K. Wickwire, J. R. Burgess, M. A. Stochelski and R. Pazdro, *Free Radical Biol. Med.*, 2014, **71**, 157–164.
5 J. Son, C. A. Lyssiotis, H. Ying, X. Wang, S. Hua, M. Ligorio, R. M. Perera, C. R. Ferrone, E. Mullarky, S. C. Ng, Y. Kang, J. B. Fleming, N. Bardeesy, J. M. Asara, M. C. Haigis, R. A. DePinho, L. C. Cantley and A. C. Kimmelman, *Nature*, 2013, **496**, 101–105.
6 S. Kolemen, M. Isik, G. M. Kim, D. Kim, H. Geng, M. Buyuktemiz, T. Karatas, X. F. Zhang, Y. Dede, J. Yoon and E. U. Akkaya, *Angew. Chem., Int. Ed.*, 2015, **54**, 5340–5344.
7 L. L. Zeng, S. Kuang, G. Y. Li, C. Z. Jin, L. N. Ji and H. Chao, *Chem. Commun.*, 2017, **53**, 1977–1980.
8 M. Daga, C. Ullio, M. Argenziano, C. Dianzani, R. Cavalli, F. Trotta, C. Ferretti, G. P. Zara, C. L. Gigliotti, E. S. Ciamporcero, P. Pettazzoni, D. Corti, S. Pizzimenti and G. Barrera, *Free Radical Biol. Med.*, 2016, **97**, 24–37.
9 E. G. Ju, K. Dong, Z. W. Chen, Z. Liu, C. Q. Liu, Y. Y. Huang, Z. Z. Wang, F. Pu, J. S. Ren and X. G. Qu, *Angew. Chem., Int. Ed.*, 2016, **55**, 11467–11471.
10 W. Tai, R. Mo, Y. Lu, T. Jiang and Z. Gu, *Biomaterials*, 2014, **35**, 7194–7203.
11 H. H. Fan, G. B. Yan, Z. L. Zhao, X. X. Hu, W. H. Zhang, H. Liu, X. Y. Fu, T. Fu, X. B. Zhang and W. H. Tan, *Angew. Chem., Int. Ed.*, 2016, **55**, 5477–5482.
12 M. Durmu and T. Nyokong, *Polyhedron*, 2007, **26**, 2767–2776.
13 G. R. Chalmers, R. M. Bustin and I. M. Power, *AAPG Bull.*, 2012, **96**, 1099–1119.
14 X. Qiu, P. Wu, L. Xu, Y. Tang and J.-M. Lee, *Adv. Mater. Interfaces*, 2015, **2**, 1500321.
15 Y. Li, W. Zhou, H. Wang, L. Xie, Y. Liang, F. Wei, J. C. Idrobo, S. J. Pennycook and H. Dai, *Nat. Nanotechnol.*, 2012, **7**, 394–400.
16 K. Ishii, *Coord. Chem. Rev.*, 2012, **256**, 1556–1568.
17 L. Zhou, W. Wang, J. Tang, J.-H. Zhou, H.-J. Jiang and J. Shen, *Chem. – Eur. J.*, 2011, **17**, 12084–12091.
18 A. Galstyan, K. Riehemann, M. Schafers and A. Faust, *J. Mater. Chem. B*, 2016, **4**, 5683–5691.
19 K. Alam, S. Ghousunnissa, S. Nair, V. L. Valluri and S. Mukhopadhyay, *J. Immunol.*, 2010, **184**, 2918–2929.
20 X. L. Chen, Y. J. Li, A. Wang, L. Zhou, S. Lu, J. H. Zhou, Y. Lin and S. H. Wei, *Dyes Pigm.*, 2015, **114**, 93–104.
21 H. Zhao, X. Cao, M. Wang, L. Tao, X. Pan, C. Yuan and W. Qian, *Nano*, 2015, **10**, 1550034.
22 W. Wang, L. Wang, Z. Li and Z. Xie, *Chem. Commun.*, 2016, **52**, 5402–5405.
23 Z. L. Pianowski, J. Karcher and K. Schneider, *Chem. Commun.*, 2016, **52**, 3143–3146.
24 J.-T. Ping, H.-S. Peng, W.-B. Duan, F.-T. You, M. Song and Y.-Q. Wang, *J. Mater. Chem. B*, 2016, **4**, 4482–4489.
25 C. Conte, F. Ungaro, G. Maglio, P. Tirino, G. Siracusano, M. T. Sciortino, N. Leone, G. Palma, A. Barbieri, C. Arra, A. Mazzaglia and F. Quaglia, *J. Controlled Release*, 2013, **167**, 40–52.
26 H. He, X. Zheng, J. Zhang, S. Liu, X. Hu and Z. Xie, *J. Mater. Chem. B*, 2017, **5**, 2491–2499.
27 E. Hachet, H. Van Den Berghe, E. Bayma, M. R. Block and R. Auzely-Velty, *Biomacromolecules*, 2012, **13**, 1818–1827.
28 Y. B. Ruan, A. F. Li, J. S. Zhao, J. S. Shen and Y. B. Jiang, *Chem. Commun.*, 2010, **46**, 4938–4940.
29 Y. Che, X. Yang and L. Zang, *Chem. Commun.*, 2008, 1413–1415, DOI: 10.1039/b719384j.
30 M. Zhang, H. N. Le, X. Q. Jiang, B. C. Yin and B. C. Ye, *Anal. Chem.*, 2013, **85**, 11665–11674.
31 D. G. He, X. X. Yang, X. X. He, K. M. Wang, X. Yang, X. He and Z. Zou, *Chem. Commun.*, 2015, **51**, 14764–14767.
32 X. M. Li, Y. J. Zheng, H. J. Tong, R. Qian, L. Zhou, G. X. Liu, Y. Tang, H. Li, K. Y. Lou and W. Wang, *Chem. – Eur. J.*, 2016, **22**, 9247–9256.
33 A. Hussain, S. Gadadhar, T. K. Goswami, A. A. Karande and A. R. Chakravarty, *Eur. J. Med. Chem.*, 2012, **50**, 319–331.
34 B. G. Ongarora, K. R. Fontenot, X. Hu, I. Sehgal, S. D. Satyanarayana-Jois and M. G. H. Vicente, *J. Med. Chem.*, 2012, **55**, 3725–3738.
35 Y. Tao, M. Li, J. Ren and X. Qu, *Chem. Soc. Rev.*, 2015, **44**, 8636–8663.
36 A. M. Durantini, L. E. Greene, R. Lincoln, S. R. Martinez and G. Cosa, *J. Am. Chem. Soc.*, 2016, **138**, 1215–1225.
37 L. Zhou, X. F. Ge, J. H. Zhou, S. H. Wei and J. Shen, *Chem. Commun.*, 2015, **51**, 421–424.
38 R. Mo, T. Y. Jiang, R. DiSanto, W. Y. Tai and Z. Gu, *Nat. Commun.*, 2014, **5**, 3364–3373.
39 J. W. Tian, L. Ding, H. X. Ju, Y. C. Yang, X. L. Li, Z. Shen, Z. Zhu, J. S. Yu and C. J. Yang, *Angew. Chem., Int. Ed.*, 2014, **53**, 9544–9549.
40 H. C. Chen, J. W. Tian, W. J. He and Z. J. Guo, *J. Am. Chem. Soc.*, 2015, **137**, 1539–1547.
41 H. Wang, B. B. Chen, S. Q. Zhu, X. X. Yu, M. He and B. Hu, *Anal. Chem.*, 2016, **88**, 796–802.
42 S. Yoon, E. W. Miller, Q. He, P. H. Do and C. J. Chang, *Angew. Chem., Int. Ed.*, 2007, **46**, 6658–6661.
43 I. Khairul, Q. Q. Wang, Y. H. Jiang, C. Wang and H. Naranmandura, *OncoTargets Ther.*, 2017, **8**, 23905–23926.

